Optical and Quantum Electronics (2023) 55:541
https://doi.org/10.1007/s11082-023-04809-6

A simulation study of quantum dot solar cells using two distinct ETL of WO_3 and WS_2

Naureen[1] · Sadanand[2] · Shambhavi Rai[1] · R. K. Yadav[2] · Pooja Lohia[3] · D. K. Dwivedi[1]

Received: 29 June 2022 / Accepted: 27 March 2023 / Published online: 15 April 2023

Abstract
Quantum dot solar cells (QDSCs) have recently attracted a lot of interest since the materials used in them are eco-friendly, good light harvesters, and cheap. Solar Cell Capacitance Simulator-1 dimensional software (SCAPS-1D) is used to carry out this numerical analysis. In the present work, the optimization of two different device architectures is investigated having WO_3 and WS_2 two different electron transport layer(ETL). In the proposed device structure, Sb_2Se_3 is used as an absorber layer and PbS is used as HTL and CdS is used as a buffer layer. The main objective of this effort is to determine how changing from the WO_3 ETL to the WS_2 ETL affects the photovoltaic parameters. Initially, the solar photovoltaic device is optimized, and then the effect of doping concentrations is investigated. In addition, the effect of series and shunt resistance on the solar device's performance is examined to illustrate the impact of series and shunt resistance on the device's performance. The effect of increasing temperature on the PV parameters is also studied and it is observed that the solar device is temperature-sensitive. Finally, the optimized performance with WS_2 ETL with PCE of 20.60% is achieved.

Keywords WO_3 · WS_2 · Quantum dot solar cell · SCAPS-1D

1 Introduction

One of the most important challenges handed to contemporary science and technology in the 21st century is the development of renewable sources of energy in order to prevent the pollution produced by the excessive use of fossil fuels and to conserve the

✉ Sadanand
sadanand2893@gmail.com

✉ D. K. Dwivedi
todkdwivedi@gmail.com

[1] Photonics and Photovoltaic Research Lab, Department of Physics and Material Science, Madan Mohan Malaviya University of Technology, Gorakhpur 273010, India

[2] Department of Applied Sciences, Galgotias College of Engineering and Technology, Greater Noida 201306, India

[3] Department of Electronics and Communication Engineering, Madan Mohan Malaviya University of Technology, Gorakhpur 273010, India

earth's biosystems. With an increase in the population, the energy demand is increasing day by day. Solar energy is an ideal option among the different renewable energy sources at the leading edge of evolving technology. Photovoltaic systems, being cost-effective and eco-friendly, has become a long-term energy source that can fulfill the energy demand. The phenomenon of the photovoltaic effect directly turns solar irradiation into energy.

Nowadays, the majority of electricity is generated by fossil fuels or nuclear power (Blaschke et al. 2013). However, these conventional sources of non-renewable energy like coal, gas, and oil are limited on earth and the demand for energy consumption is increasing day by day with the development of technology and increasing population (Tripathi et al. 2020; Bhardwaj et al. 2021). Thus, to accomplish the requirements of clean and free energy, renewable energy sources have received a lot of attention (Sadanand and Dwivedi 2019a). The sun itself is a source of a vast amount of energy that has the ability to accommodate the energy and electricity requirements of the world. Therefore, to utilize the sun's energy, solar cell technology should be made available (Sadanand and Dwivedi 2020a; Kumar et al. 2018).

To have an efficient performance of photovoltaic cells, researchers are working in different fields and the third-generation quantum dot solar cell (QDSCs) is one of the promising candidate because of its adjustable bandgap size, small size (less than exciton Bohr radius), and specific optoelectronic properties (Yuan et al. 2020; Gao et al. 2018; Emin et al. 2011; Sukharevska et al. 2021). For efficient utilization of high energy radiations, lately, the multi-exciton generation effect has been reported in QDSCs (Tvrdy and Kamat 2011). Generally, TiO_2, ZnO, etc. have been employed as ETL material in QDSCs due to their high dielectric constant for exciton detachment and appropriate energy levels. Because of astonishing properties such as high melting point (1,473 °C), good anti-reflection nature, wider band gap, etc. Tungsten trioxide (WO_3) seems to be a new ETL material. A QDSC is a nanometer-scaled photoelectric semiconductor crystal (Kramer and Sargent 2014) that converts the light energy from sunlight into electrical energy (Sharma et al. 2019).

QDSCs are attracting the attention of researchers all around the world because of their cost-effectiveness (Guo et al. 2017) and compact structure. QDSCs having a "sandwich" type structure are comprised of three layers: electron transport layer (ETL), hole transport layer (HTL), and the absorber layer. The extinction coefficient and absorption spectrum of quantum dots may be readily controlled by the material size. The quantum confinement effect allows the bandgap to be modified by changing the size of QDs (Chen et al. 2021). Despite all of these tremendous efforts up to date, the QDSCs' efficiency remains quite low, necessitating a large amount of effort to reach its theoretical highest value. The lower value of the efficiency of the solar device is due to the lower charge carrier concentrations and their mobility. As a result, several materials for various layers are being researched to develop a significantly more efficient and practical device (Rühle et al. 2010).

In this work, we have designed a device structure with different ETL materials in order to have more efficient solar device. A QDSC device is designed using appropriate HTL materials, as illustrated in Fig. 1a, b. Materials for various layers comprises WO_3 as an ETL, CdS as the buffer layer, Sb_2Se_3 for the absorber, and PbS-EDT is used for the HTL. When it comes to improving the functionality of the QDSCs, ETL plays a crucial role. As a result, researchers are searching for the optimum photovoltaic material that can enhance PCE and lower the cost of the solar cell device. In this study, after the device is properly designed and calibrated, the WO_3 ETL materials are changed by WS_2

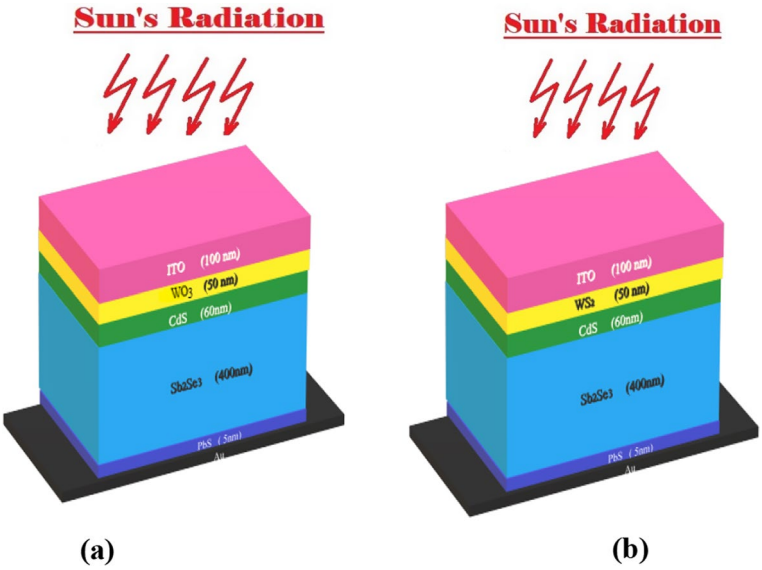

Fig. 1 The device structure of the solar photovoltaic cell having **a** WO_3 as ETL and **b** WS_2 as ETL

ETL material, and an in-depth examination is undertaken. The results for distinct P–V parameters such as Jsc(mA/cm^2), Voc(V), FF(%), and PCE(%), as well as the current density and voltage (J-V) curve, are displayed with the aid of graphs.

The work is divided into four sections. Section 1 gives an overview of the quantum dot solar cell device. The operating and layered architecture of QDSCs are discussed in Sect. 2. The impact of ETL replacement, as well as the doping, resistance, and temperature analysis of both devices, are discussed in Sect. 3. J-V curve and a comparative study of the impacts of PV parameters are performed. Along with the J-V curve, an ETL analysis is done to illustrate the effect of parameter modification on the devices. The present work comes to an end in the fourth part, Sect. 4.

2 Device structure and material parameters

The theoretical analysis is carried out in this work to enhance the performance of solar photovoltaic cells with WO_3 as ETL and WS_2 as ETL (Sadanand and Dwivedi 2019b). The efficiency of the solar device is studied using the SCAPS-1D numerical simulation program software for solar cell capacitance (Sadanand and Dwivedi 2019b). Simulation software is a significant tool for estimating the performance of solar cell devices and for connecting the practical and theoretical production of solar cells (Sadanand et al. 2021). Figure 1a illustrates the construction of a solar photovoltaic device, having different layers as ITO/WO_3/CdS/Sb_2Se_3/PbS/Au. Here, the WO_3 layer is employed as an electron transport layer (ETL) which is coupled with the Indium doped Tin Oxide (ITO) layer through which the light enters the device. CdS is used as the buffer layer, Sb_2Se_3 as the absorber layer, and PbS-EDT is employed as HTL. Gold (Au) acts as the back contact through which PbS-EDT is coupled. In Fig. 1b, the WO_3 ETL has been replaced with WS_2. The calibrated layers are used to analyze the device structure ITO/WO_3/CdS/Sb_2Se_3/PbS-EDT/Au and the

Table 1 Solar cell device parameter of different layers used for analysis (Tamilselvan, Muthusamy, et al. 2018; Rai et al. 2020)

Parameters	ITO	WS_2	WO_3	CdS	Sb_2Se_3	HTL
Thickness(nm)	25	50	50	60	400	5
E_g(eV)	3.5	1.8	2.0	2.4	1.06	1.2
Affinity for Electrons (eV)	4.0	3.95	3.8	4	4.15	4.0
Dielectric permittivity	9.0	13.6	4.8	10	19	10
Electrons' Mobility μ_e (cm^2/Vs)	20	100	30	100	10	0.01
Holes' Mobility μ_h (cm^2/Vs)	10	100	30	25	1	0.01
N_D (cm^{-3})	1×10^{18}	1.0×10^{18}	6.35×10^{17}	1.1×10^{18}	-	1×10^{15}
N_A (cm^{-3})	–	–	–	–	2×10^{14}	1.00×10^{15}
N_t (cm^{-3})	10^{14}	10^{15}	10^{15}	10^{14}	10^{14}	1.0×10^{14}
N_c (cm^{-3})	2.2×10^{18}	2.2×10^{17}	2.2×10^{21}	2.2×10^{18}	1.0×10^{18}	1.0×10^{19}
Nv (cm^{-3})	1.8×10^{18}	2.2×10^{16}	2.2×10^{21}	1.8×10^{19}	1.8×10^{20}	1.8×10^{13}
Thermal velocity of e^- (cm/s)	10^7	10^7	10^7	10^7	10^7	10^7
Thermal velocity of holes (cm/s)	1.0×10^7	1.0×10^7	1.0×10^7	1.0×10^7	1.0×10^7	1.0×10^7

Table 2 The CdS trap states parameter for SCAPS simulation (Rai et al. 2020)

Parameter	Defect 1
Type of defect	Single acceptor (-/0)
E_t (eV) above E_v	1.2
Electron capture cross section (cm^2)	1.0×10^{-17}
Hole capture cross section(cm^2)	1.0×10^{-12}
N_t(cm^{-3})	1.0×10^{-18}

new improved solar device comprises of WS_2 as ETL. WS_2 material has an advantage over WO_3 material which includes high melting point, photoelectrochromic, mechanical properties, and toughness. Because of these properties, WS_2 is considered as a promising applicant for electrical and optical applications. Further, tungsten disulfide has the ability to provide good resistance against corrosion.

As the solar radiation falls on the solar cell device, the energy of the radiation gets engrossed by the active layer which generates charge carriers (Prasad et al. 2021). The absorber layer (Sb_2Se_3), sandwiched between the electron transport layer (ETL) and hole transport layer (HTL) is the most important layer because it converts the light energy directly into electrical energy. It separates the oppositely charged carriers (electrons and holes) with the help of internal electro-chemical potential. Charge carriers are thus transported to ETL and HTL respectively. The buffer layer is coupled with the absorber layer to ensure that most of the radiation get absorbed at the junction (Pandey et al. 2021; Zhang et al. 2012).

Tables 1, 2, and 3 provide all of the parameters utilized in the SCAPS-1D simulator to design the device. The operating temperature is set to 300 K for simulation reasons, with shunt and series resistances of 10^6 Ω and 1 Ω, respectively. The quantum dot solar cell is illuminated with an Air Mass (AM) of 1.5 sunlight and a global spectrum (1000 Wbm^{-2}) (Sadanand and Dwivedi 2020b, 2021).

Table 3 The Sb_2Se_3 trap states parameter for SCAPS simulation (Rai et al. 2020)

Parameter	Defect 1
Type of defect	Neutral
E_t (eV) above E_v	0.55
Electron capture cross section (cm^2)	1.0×10^{-13}
Hole capture cross section (cm^2)	1.5×10^{-14}
N_t (cm^{-3})	1.6×10^{-15}

The Solar Cell Capacitance Simulator (SCAPS-1D) is a solar device simulator application created by the Department of Electronics and Information Systems at the University of Gent (ELIS) (Rai et al. 2021). This simulator allows us to construct up to seven semiconductor layers, defects inside each layer, and defects between two layers' interfaces, as well as compute and visualize I-V parameters, energy band, PV parameters, J-V, and other parameters. Using this SCAPS-1D simulator, a comparison between the device with as WO_3 as ETL and the device with WS_2 as HTL is performed and discussed in the forthcoming section-4 below.

The Poisson and continuity equations were the fundamental equations that have been employed during the SCAPS-1D simulation. These equations can be mathematically represented as follows:

Poisson Equation (Prasad et al. 2021):

$$\frac{\partial}{\partial x}\left(\varepsilon_0\varepsilon\frac{d\psi}{dx}\right) = -q\left[-n + p - N_A^- + N_D^+ - n_t + p_t\right] \tag{1}$$

where q represents the electronic charge; ψ represents the electrostatic potential; p represents the unbounded holes; n represents unbounded electrons; n_t represents the trapped electrons; p_t represents trapped holes; N_A^-, N_D^+ represents the ionized donor like doping and ionized acceptor like doping respectively;ε represents the permittivity and ε_0 permittivity of free space.

The Continuity Equations (Prasad et al. 2021):

$$\left(\begin{array}{l} -\frac{\partial J_n}{\partial x} + G\cdot U_n = \frac{\partial n}{\partial t} \\ -\frac{\partial J_p}{\partial x} + G\cdot U_p = \frac{\partial p}{\partial t} \end{array}\right)\left\{\begin{array}{l} J_n = -\frac{\mu_n}{q}n\frac{\partial E_{Fn}}{\partial x} \\ J_p = +\frac{\mu_p}{q}p\frac{\partial E_{Fp}}{\partial x} \end{array}\right.$$

where J_p represents the current density of holes; J_n represents the current density of electrons; G represents the generation rate; μ_p represents the mobility of holes; μ_n represents the mobility of electrons, U_p represents the combination rate of holes, U_n represents the recombination rate of electrons; E_{Fn} represents the electron quasi-Fermi level and E_{Fp} represents the hole quasi-Fermi level.

These coupled differential equations are solved by the SCAPS-1D simulator. It solves and calculates the values of unidentified variables.

3 Result and Discussion

This section includes the outcome of all the analysis that have been performed in the current work. This particular section is divided in six subsections, each discuss different aspect of the investigation.

3.1 Comparative study on the influence of replacement of the ETL

The calibration of the device and the examination of ETL replacement are discussed in this sub-section of the result. The solar device was designed and calibrated using the simulator SCAPS-1D. A schematic device construction is created first having WO_3 as ETL with 50 nm of thickness. The other layers have CdS as having the thickness of 60 nm, Sb_2Se_3 is used as having a thickness of 400 nm and PbS-EDT as HTL having 5 nm thickness. CdS is used as buffer layer, Sb_2Se_3 is used as absorber layer and PbS as HTL. Initially the optimization of the device has been done followed by an analysis on the acceptor doping concentration. The other layers include CdS as buffer layer having the thickness of 60 nm, Sb_2Se_3 as the absorber layer having a of thickness 400 nm, and PbS-EDT as HTL having the thickness of 5 nm. After successfully calibrating the device, WO_3 is replaced with WS_2 material. The thickness of both the material is kept constant to have more balanced analysis. To investigate the effect of this replacement of ETL on the photovoltaic parameters energy band diagram (EBD), the external quantum efficiency (EQE), and current density and voltage (J-V) curve are used, as illustrated in Figs. 2, 3 and 4.

The bandgap of a semiconductor is directly correlated to the Voc of the solar device. WO_3 have a bandgap of 2.0 eV which is slightly larger in comparison to the band gap of WS_2 having bandgap of 1.8 eV. In the Fig. 2 the spike of WO_3 is different from that of WS_2 because of the replacement of n-type semiconductor material by keeping the same p-type material. Because of this replacement of n-type material the level of valance band and conduction band will transform after p–n junction formation.

A quantum dot solar cell's quantum efficiency is the amount of current it produces when the photons of certain wavelength is irradiated on it. Within the wavelength range of 300–1300 nm, the QE curve of the PCE for the device with WO_3 and WS_2 as ETL layers is shown in Fig. 3. With distinct ETLs on both devices, the QE value is greater than

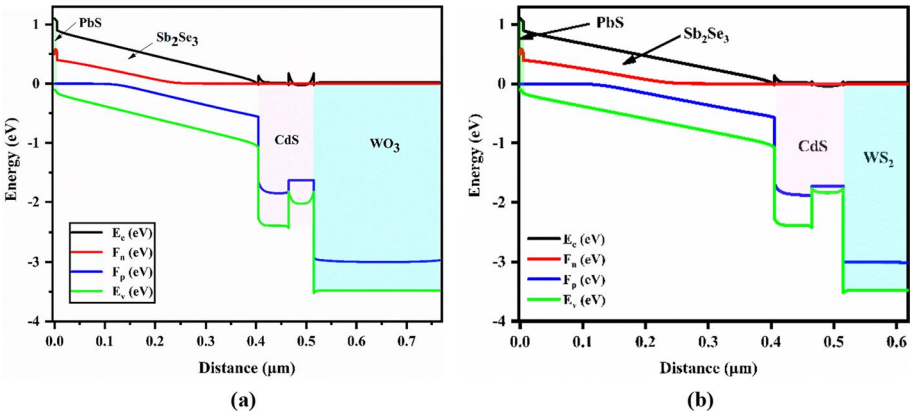

Fig. 2 Energy band diagram of the solar device having **a** WO_3 and **b** WS_2 as ETLs

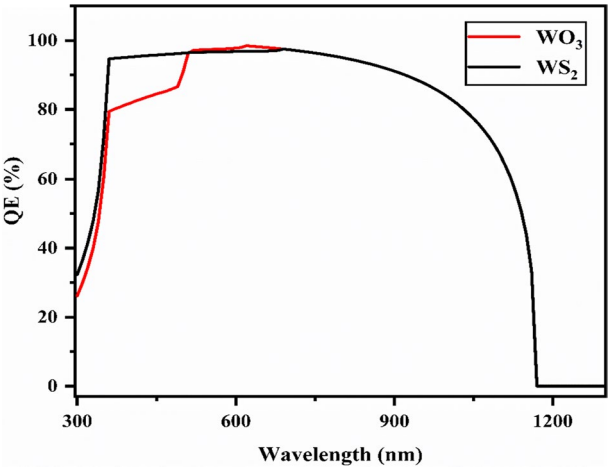

Fig. 3 EQE of WO_3 ETL and WS_2 ETL based solar device

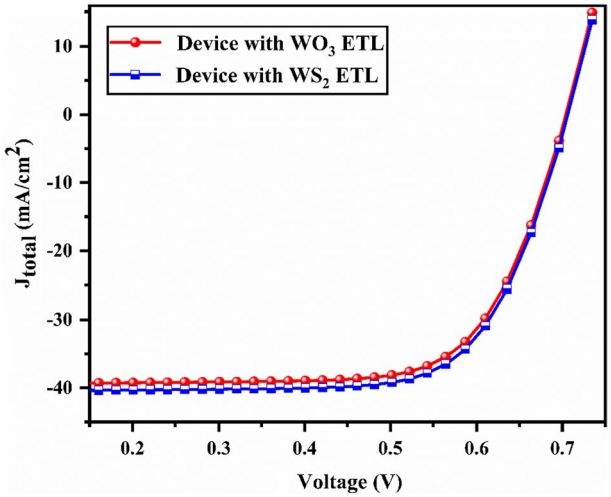

Fig. 4 J-V Curve of WO_3 and WS_2 ETL based solar cell

Table 4 Photovoltaic parameters of the device having WO_3 as ETL, device having WS_2 as ETL and the certified device (Chen et al. 2017)

Solar Device	J_{sc} (mA/cm^2)	V_{oc} (V)	FF (%)	PCE (%)	References
WO_3 ETL based solar device	39.45	0.704	72.09	20.05	This work
WS_2 ETL based solar device	40.52	0.706	72.00	20.60	This work
PbS CQD HTL (certified)	25.5	0.427	59.3	6.50	Chen et al. 2017)
Cu2O HTL based QDSC device	24.60	0.7559	73.76	13.72	Prasad et al. 2021)
Zn – Cu – In – Se QDSCs (Certified value)	25.25	0.739	62.2	11.61	Du et al. 2016)
TiO_2 ETL based device	24.46	0.635	63.8	9.87	Ray et al. 2021)

Table 5 Summary of solar devices with Sb2Se3 as absorbser layer with various ETLs and HTLs

Device Structure	ETL	HTL	PCE (%)	References
ITO/WO_3/CdS/Sb_2Se_3/PbS/Au	WO_3	PbS	20.05	This work
ITO/WS_2/CdS/Sb_2Se_3/PbS/Au	WS_2	PbS	20.60	This work
ITO / In2S3/Sb2Se3/Cu2O/CNT	/	Cu2O	13.20	Baig et al. 2019)
ITO/CdS/Sb2Se3/PbS colloidal quantum dots (CQDs)/Au	CdS	PbS CQDs	6.50	Chen et al. 2017)

90%. The quantum efficiency value improves with the increase in wavelength from 350 to 400 nm. After that, it remains nearly constant up to 800 nm before gradually decreasing to 1150 nm. The reason behind this gradual decrease is the reflection of radiations from the solar device's surface. After 1150 nm, both the devices exhibit zero external quantum efficiency (EQE). The current density and voltage (J-V) curve for different ETL layers was obtained by simulation of the data given in Table 1 and is depicted in Fig. 4. J-V curve is considered an important technique because it helps to obtain the photovoltaic parameters such as Jsc, Voc, FF an,d PCE of the solar devices. Table 4 represents a comparison between the output data for both of the devices. The Jsc value for WS_2 ETL was attained to be 40.52 mA/cm^2 which is higher than that of WO_3 having the J_{sc} of 39.45 mA/cm^2. Further, the WS_2 ETL-based QDSC showed the optimum efficiency of 20.60% which is higher than the efficiency obtained by WS_2 ETL-based QDSC having the PCE of 20.05%. Table 5 shows the efficiency of photovoltaic devices having Sb_2Se_3 as the absorber layer with different ETL and HTL.

3.2 Impact of variation of acceptor density of HTL Layer

In this sub-section, the influence of doping concentration of the HTL on the performance of the device has been studied. The analysis is done by varying the acceptor doping concentration from 1×10^{15} to 1×10^{20} cm^{-3} in five equal steps along *x*-axis while keeping other parameters constant. All the parameter's value mentioned above were entered in SCAPS-1D simulator. The attained outcomes were illustrated in Fig. 5a–d. From the Fig. 5a–d it is seen that the device parameters like Fill factor (FF), power conversion efficiency (PCE) and open circuit voltage (V_{OC}) increases for both of the devices as the doping concentration of HTL is increased whereas J_{SC} almost remains constant for both of the devices with increasing acceptor density concentration.

From the Fig. 5a–d, it has been observed that by varying the doping density of PbS-EDT HTL, the performance of the device having WS_2 as ETL is better than the solar device having WO_3 as ETL. Figure 5a shows a comparison for the power conversion efficiency (PCE) of both devices. Solar device having WO_3 as ETL has a maximum efficiency of 20.11% at 1×10^{22} cm^{-3} whereas for WS_2 ETL based device maximum PCE obtained is 20.67% at 1×10^{22} cm^{-3}. PCE of the device is the most important photovoltaic parameter because it displays the solar cell ability to convert the light energy into electrical energy. Comparative study for the Jsc of both of the solar devices is represented in Fig. 5b. It has been observed that the short circuit current density Jsc of both the devices is almost constant. However, the J_{sc} for WS_2 ETL based device is higher than the Jsc for WS_2 ETL based device. Device having WO_3 as ETL has a maximum Jsc of 39.45 mA/cm^2 whereas for WS_2 ETL based device maximum Jsc obtained is 40.52 mA/cm^2.

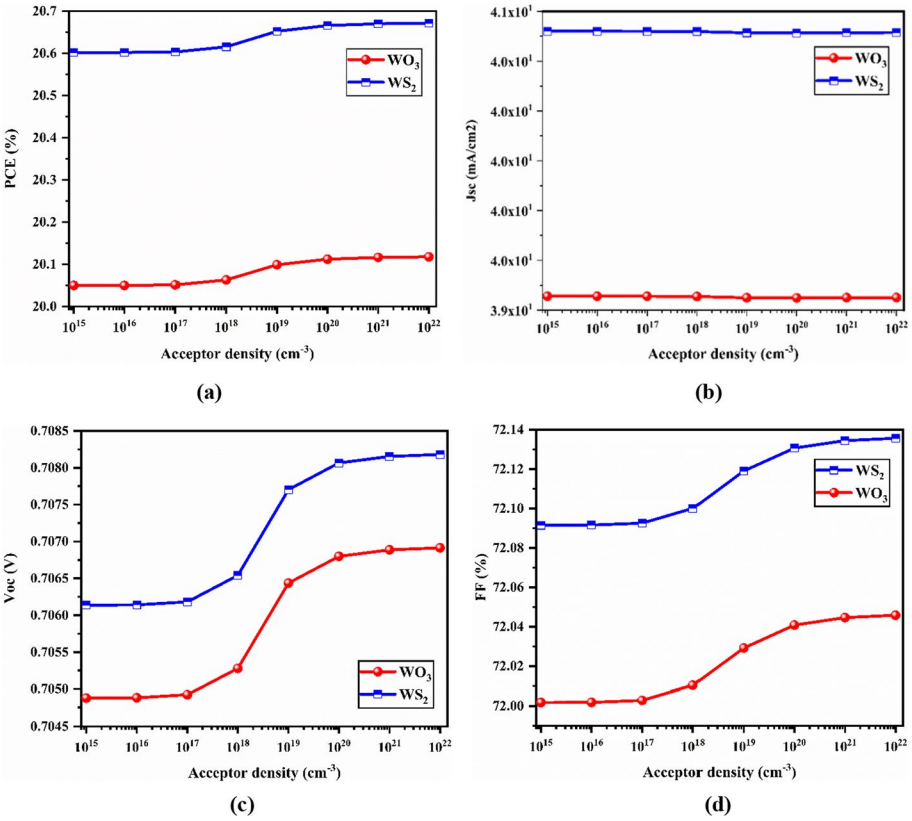

Fig. 5 Influence of acceptor density of HTL on **a** PCE, **b** Jsc, **c** Voc, and **d** FF for WO_3 ETL and WS_2 ETL based devices

The maximum Voc obtained by WO_3 and WS_2 ETL based device is 39.45 V and 40.52 V at 1×10^{15} cm^{-3} respectively and is depicted in Fig. 5c. The fill factor of the device is increased from 72.09 to 72.13% for WO_3 ETL based device and from 72.00 to 72.04% for WS_2 ETL based device, as the acceptor doping concentration is varied from 1×10^{15} to 1×10^{22} cm^{-3}. The best value of fill factor (FF) is obtained at the doping concentration of 1×10^{22} cm^{-3}. The FF generated is lower because of the reduced conductivity of WS_2 ETL based devices. As a result, the charge carriers produced by the solar device is decreased. Hence, the optimum FF value is achieved when the doping density is less than 1×10^{22} cm^{-3}.

3.3 Influence of resistance on the photovoltaic parameters

In this sub-section, the influence of resistance on P–V parameters such as power conversion efficiency (PCE) and fill factor (FF) of the solar device is studied and depicted in Fig. 6a–d. The performance of solar cells is heavily influenced by resistance. In theory, any idealized solar photovoltaic device has a series resistance of zero ohm and shunt resistance of infinity, but in practice things aren't that concise. When the current travels between the two electrical contacts, every device has some resistance, and solar devices have losses due to

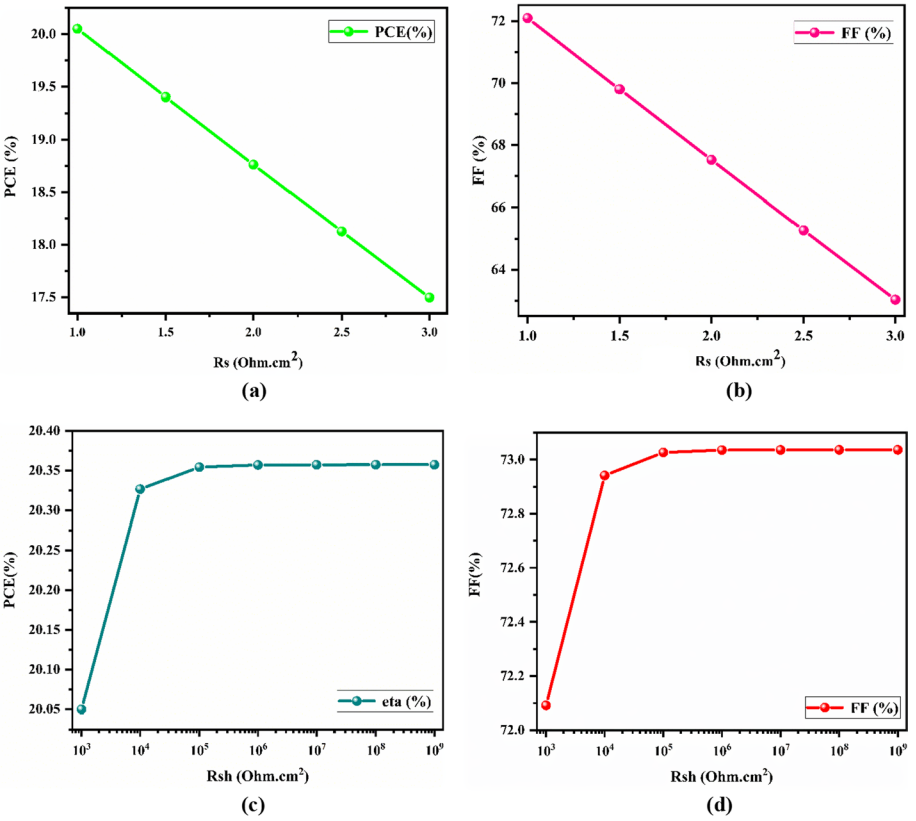

Fig. 6 Impact of resistance variation on **a** power conversion efficiency (PCE) for series resistance and **b** fill factor (FF) for series resistance; **c** PCE for shunt resistance and **d** FF for shunt resistance

material resistance (Rs). Series and shunt resistances of solar photovoltaic cells are intrinsic factors which represent losses (Pandey et al. 2020). The two photovoltaic characteristics most impacted by series and shunt losses are the fill factor and efficiency (Paquin et al. 2015). Figure 6a,b represents the analysis of series resistance for the WS_2 ETL-based solar device. Series resistance decreases the FF of the solar device. It also influences and reduces the short circuit current (Isc) of the solar device. From the graph, it has been observed that, as the series resistance increases from 1.0 Ohm cm^2 to 3.0 Ω cm^2 the values of PCE and FF decrease from 20.04 to 17.49% and from 72.09 to 63.03% respectively. Since few resistance is present in the solar device, the best value of both the PV parameters is obtained at 1.0 Ohm cm^2. Shunt resistance (Rsh) is also important for enhancing solar cell performance, and it can be caused by manufacturing defects (Chen et al. 2021; Rühle et al. 2010). Figure 6c,d represents the shunt resistance for WS_2 ETL-based device. From the graph, it has been observed that the power conversion efficiency (PCE) and fill factor (FF) of the device rises up to a certain point and then become constant. The best value is obtained at 1×10^9 Ohm cm^2 and the values of PCE and FF at that value of shunt resistance are 20.35 and 73.03% respectively. The lower value of shunt resistance degrades the performance of the solar device by providing an alternative way for the photo-generated current. \

3.4 Influence of temperature on PV parameters

In the present sub-section, the impact of temperature on the efficiency of the solar cell has been discussed. Solar devices are installed in an open area and are exposed to the sun. Higher temperature is a cause of concern in some areas where the temperature is too high. Higher temperature causes a decrease in the efficiency and all other photovoltaic parameters of the device (Xing et al. 2020; Kirmani et al. 2018). Figure 7 represents the influence of temperature on the efficiency of the device. The temperature has been varied from 300 to 500 K for both of the devices at a step of 50 K. From the Fig. 7, it has been observed that the efficiency of both the devices decreases with the increase in temperature. Throughout the simulation, the thickness of both of the ETLs is kept constant at 50 nm. The PCE of the WO_3 ETL based solar cell device, at 300 K, is 20.04% and the WS_2 ETL-based device is 20.60%. At 500 K, the PCE of the WO_3 ETL-based device and WS_2 ETL-based device has become 7.79 and 8.11% respectively. All other photovoltaic parameters also decrease with the increase in temperature. The reason behind this linear decrement in the photovoltaic parameters is the increase in reverse saturation current of the device.

3.5 Influence of thickness of ETL on PV parameters

The ETL and HTL are responsible for several vital tasks in the operation and performance of solar devices (Rai et al. 2020). They are responsible for the charge transfer function, as well as the light absorption process. As a result, the thickness of their layers in a solar cell arrangement affects charge carrier synthesis, transportation, and the overall performance of the photovoltaic device (Sadanand and Dwivedi 2019b; Sadanand et al. 2021).

In the present sub-section the effect of ETL thickness on the photovoltaic parameters of the solar cell have been investigtated and represented in Fig. 8a-d. The thickness of ETL material for both the devices has been varied from 40 to 90 nm by keeping all other parameters like bandgap and thickness of HTL and absorber layer constant. It has been observed that on varying the thickness of ETL the photovoltaic parameters such as power conversion efficiency (PCE), open-circuit voltage (Voc) and short circuit current density (Jsc)

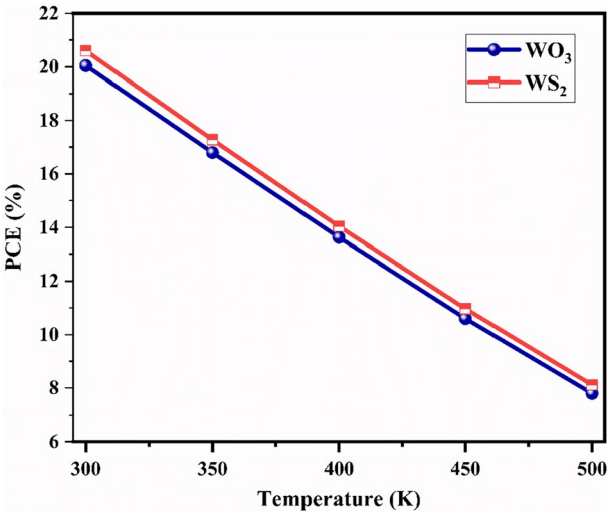

Fig. 7 Impact of increasing temperature on the QDSC device performance

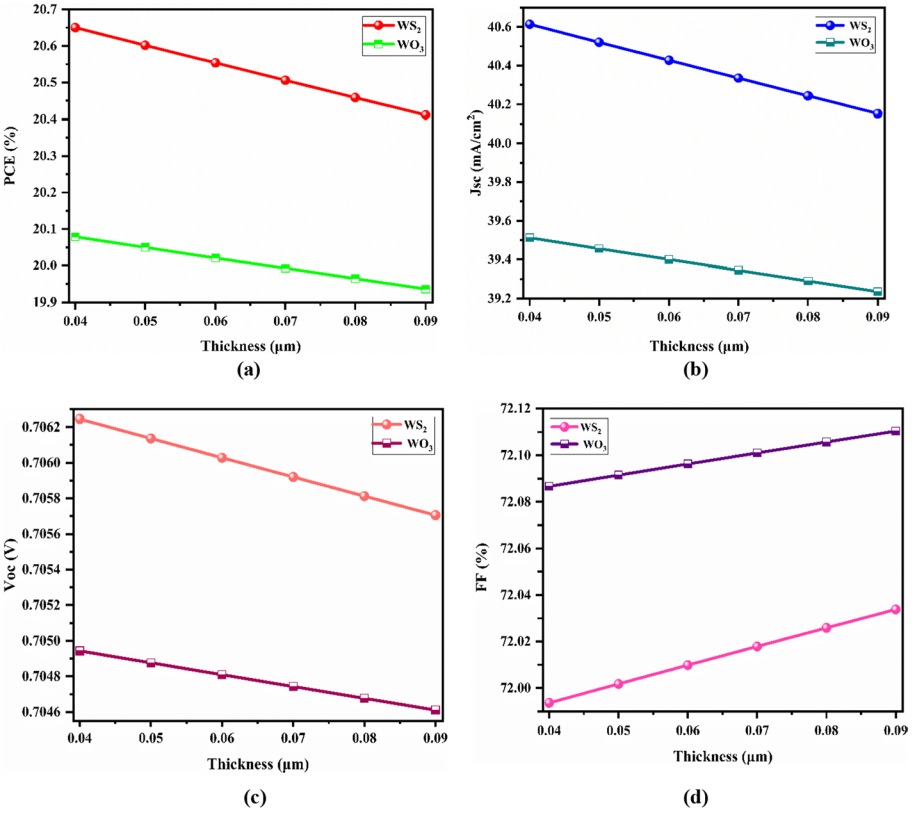

Fig. 8 Impact of increasing thickness on **a** power conversion efficiency (PCE), **b** short-circuit current density (Jsc), **c** open circuit voltage (Voc) and **d** fill factor (FF) of the photovoltaic device

decreases for both WO_3 and WS_2 ETL based device. It occurs due to the recombination of charge carriers and less generation of electron–hole pairs (Rai et al. 2020). It means that as the thickness of the ETL increases, the electrons and holes generations decreases and consequently it reduces the output efficiency of the device. However, the fill factor of the device decreases as the thickness of ETL decreases. At 40 nm of thickness, the PCE, Voc, Jsc, and FF of WO_3 ETL based solar device is 20.07%, 0.70 V, 39.51 mA/cm^2 and 72.08% respectively and that for WS_2 ETL based solar device is 20.65%, 0.70 V, 40.61 mA/cm^2 and 71.99364% respectively. As the thickness of the device increases up to 90 nm, the value of PCE, Voc, Jsc and FF of WO_3 ETL based device becomes 19.93%, 0.704 V, 39.23 mA/cm^2 and 72.11% respectively and that for WS_2 ETL based solar device is 20.41%, 0.70 V, 40.15 mA/cm^2 and 72.03% respectively.

3.6 ETL defect density

The creation of charge carriers and their recombination are the two essential characteristics that regulate the solar cell's performance. When the device is illuminated, there is generation of charge carriers which dissociate and are collected by the corresponding electrodes before being transported to the external circuitry. Due to the low film quality and

bulk defect density in the absorber, recombination may occur during the charge collecting process of these light produced carriers (Sahu et al. 2020). As a result, the overall defect density of the WO_3 ETL and that of WS_2 ETL was altered from 1×10^{11} to 1×10^{19} cm^{-3} to examine the acceptable range of these defects for the most efficient device and is represented in Fig. 9a–d. From the Fig. 9a–d it has been observed that the values of all the photovoltaic parameters such as Voc, PCE and Jsc decreases with the increase in defect density but the fill factor (FF) for both of the device increases. The reason behind this degradation is that as the defect density increases the rate of recombination due to higher pinholes, and the rate of film deterioration is likewise higher. As a result, the device's stability and overall performance degrade (Yasin et al. 2021). As compared to the values obtained at the initial defect density input, the solar cell's performance is considerably improved with PCE of 20.59%, Jsc of 40.50 mA/cm^2, Voc of 0.70 V, and FF of 72.00% at a low defect density of 1×10^{11} cm^{-3} for WO_3 ETL based device and for WS2 ETL based device the values of PCE, Jsc, Voc and FF are 20.67%, 40.66 mA/cm^2, 0.70 V and 71.98% respectively.

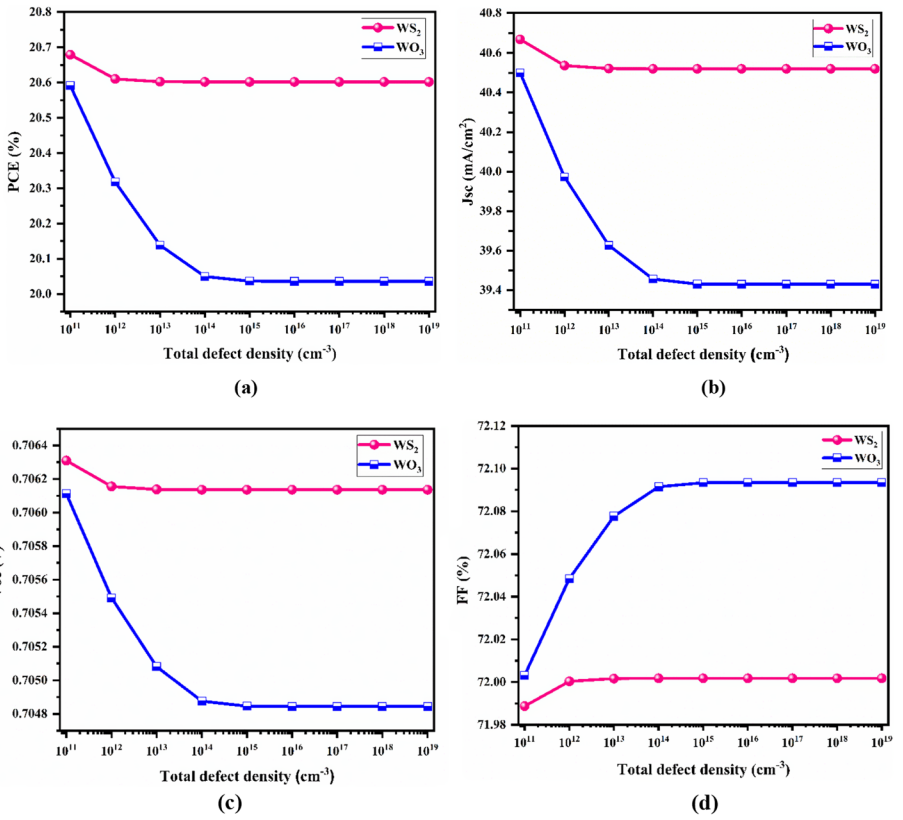

Fig. 9 Impact of increasing the defect density of WO_3 and WS_2 ETL based device on **a** power conversion efficiency (PCE), **b** Short-circuit current density (Jsc), **c** Open circuit voltage (Voc) and **d** Fill factor (FF) of the photovoltaic device

4 Conclusion

The simulation of quantum dot solar cells (QDSCs) using various ETL materials have been carried out and WS_2 as an ETL material seems to be most suitable material as an electron transport layer (ETL) in comparison to the WO_3 as an ETL. The energy band diagram, J-V characteristics and EQE for both of the devices have been investigated. The impact of acceptor density of HTL, resistance, and temperature on the photovoltaic parametes of the solar device have also been studied in detail. It could be concluded that both the solar devices are very sensitive to temperature. The rise in the temperature of the QDSCs reduces the conductivity of the material which in turn degrades the photovoltaic parameters. Also, the increase in thickness and defect density of ETL material of both the solar device causes reduction in the performance of the solar device. The photovoltaic parameters such as J_{sc}, V_{oc}, FF and PCE for the WS_2 ETL based device are 40.52 mA/cm^2, 0.706 V, 72.00 and 20.60% respectively. Using optimum values of the solar parameters it has been observed that (1) WS_2 as an ETL gives better PCE as compared to WO_3 as ETL; (2) On increasing the acceptor desitity of the HTL, the photovoltaic parameters such as V_{oc}(V), FF(%), PCE(%) increases for both of the devices however the PV parameters of the device having WS_2 as ETL is higher than that of WO_3 as ETL (3) the best output of the PV parameters is obtained at the value of 1.0 Ω cm^2 of the series resistance; (iv)At 1×10^9 Ω cm^2 value of the shunt resistance, maximum efficiency of the device is obtained. The results of the present study also be further used to increase the performance of the WS_2 ETL based QDSC by optimising and analysing the ETL/HTL/absorber concentration and defects at interface. The simulation performed in the current study will help the researchers to design and optimize novel ETL layer thereby improving the performance of the QDSC device.

Acknowledgements Authors are thankful to Madan mohan Malaviya University of Technology, Gorakhpur for providing the support to carry out this work.

Author contributions N, S and SR analyze the device structure, simulation study and drafted the manuscript. RKY, PL and DKD updated the draft file of manuscript.

Funding No funding available for the proposed work.

Data availability There is no additional data available for the proposed work.

Code availability There is no code available for the proposed work.

Declarations

Conflict of interest We all the authors confrms that there is no conflict of interest.

Ethics approval No ethics approval is required for proposed work.

Consent to participate For proposed work no consent to participate is required.

Consent for publication We all the authors are agree to publish the manuscript content. The proposed work is original and have not submitted or considered for publication elsewhere.

References

Baig, F., Khattak, Y.H., Beg, S., Soucase, B.M.: Numerical analysis of a novel CNT/Cu2O/Sb2Se3/In2S3/ITO antimony selenide solar cell. Optik (Stuttg). **197**, 163107–163114 (2019)

Bhardwaj, K.S., Rai, S., Lohia, P., Dwivedi, D.K.: Investigating the performance of mixed cation mixed halide-based perovskite solar cells using various hole-transport materials by numerical simulation. Opt. Quantum Electron **53**(11), 1–16 (2021)

Blaschke, T., Biberacher, M., Gadocha, S., Schardinger, I.: 'Energy landscapes': Meeting energy demands andhuman aspirations. Biomass Bioenerg. **55**, 3–16 (2013)

Chen, C., et al.: 6.5% certified efficiency Sb_2Se_3 solar cells using PbS colloidal quantum dot film as hole-transporting layer. ACS Energy Lett. **2**(9), 2125–2132 (2017)

Chen, J., Jia, D., Johansson, E.M.J., Hagfeldt, A., Zhang, X.: Emerging perovskite quantum dot solar cells: feasible approaches to boost performance. Energy Environ. Sci. **14**(1), 224–261 (2021)

Du, J., et al.: Zn-Cu-In-Se quantum dot solar cells with a certified power conversion efficiency of 11.6%. J. Am. Chem. Soc **138**(12), 4201–4209 (2016)

Emin, S., Singh, S.P., Han, L., Satoh, N., Islam, A.: Colloidal quantum dot solar cells. Sol. Energy **85**(6), 1264–1282 (2011)

Gao, W., et al.: Towards understanding the initial performance improvement of PbS quantum dot solar cells upon short-term air exposure. RSC Adv. **8**(27), 15149–15157 (2018)

Guo, Y., et al.: Single phase, high hole mobility Cu_2O films as an efficient and robust hole transporting layer for organic solar cells. J. Mater. Chem. A **5**(22), 11055–11062 (2017)

Kirmani, A.R., et al.: Overcoming the ambient manufacturability-scalability-performance bottleneck in colloidal quantum dot photovoltaics. Adv. Mater. **30**(35), 1–9 (2018)

Kramer, I.J., Sargent, E.H.: The architecture of colloidal quantum dot solar cells: materials to devices. Chem. Rev. **114**(1), 863–882 (2014)

Kumar, M.S., Madhusudanan, S.P., Batabyal, S.K.: Substitution of Zn in earth-abundant Cu2ZnSn(S, Se)4 based thin film solar cells – a status review. Sol. Energy Mater. Sol. Cells **185**, 287–299 (2018)

Tamilselvan, Muthusamy, and Bhattacharyya, Aninda J. "Tetrahedrite (Cu12Sb4S13) ternary inorganic hole conductor for ambient processed stable perovskite solar cells." ACS Applied Energy Materials 1(8), 4227–4234 (2018)

Pandey, R., Khanna, A., Singh, K., Patel, S.K., Singh, H., Madan, J.: Device simulations: toward the design of >13% efficient PbS colloidal quantum dot solar cell. Sol. Energy **207**, 893–902 (2020)

Pandey, S., Sadanand, Singh, P.K., Lohia, P., Dwivedi, D.K.: Numerical studies of optimising various buffer layers to enhance the performance of tin sulfide (SnS)-based solar cells. Trans. Electr. Electron. Mater. **22**(6), 893–903 (2021)

Paquin, F., Rivnay, J., Salleo, A., Stingelin, N., Silva, C.: Multi-phase semicrystalline microstructures drive exciton dissociation in neat plastic semiconductors. J. Mater. Chem. C **3**, 10715–10722 (2015)

Prasad, S., Sadanand, Lohia, P., Dwivedi, D.K.: Efficient PbS colloidal quantum dot solar cells employing Cu2O as hole transport layer. Opt. Quantum Electron. **53**(8), 1–14 (2021)

Rai, N., Rai, S., Singh, P.K., Lohia, P., Dwivedi, D.K.: Analysis of various ETL materials for an efficient perovskite solar cell by numerical simulation. J. Mater. Sci. Mater. Electron. **31**(19), 16269–16280 (2020)

Rai, S., Pandey, B.K., Garg, A., Dwivedi, D.K.: Hole transporting layer optimization for an efficient lead-free double perovskite solar cell by numerical simulation. Opt. Mater. Amst. **2021**(121), 111645–111657 (2021)

Ray, S., Lohia, S.P., Dwivedi, D.K.: Engineering in SnS-based solar cell for an efficient device with nickel oxide (NiO) as the hole transport layer. Adv. Mater. Lett. **12**(9), 1–1 (2021)

Rühle, S., Shalom, M., Zaban, A.: Quantum-dot-sensitized solar cells. ChemPhysChem **11**(11), 2290–2304 (2010)

Sadanand, Dwivedi, D.K.: Theoretical investigation on enhancement of output performance of CZTSSe based solar cell. Sol. Energy. **193**, 442–451 (2019)

Sadanand, Dwivedi, D.K.: Theoretical investigation on enhancement of output performance of CZTSSe based solar cell. Sol. Energy **193**, 442–451 (2019)

Sadanand, Dwivedi, D.K.: Theoretical investigation to enhance the performance of CZTSSe solar cell via back surface field. AIP Conf. Proc **2220**, 140009–140014 (2020)

Sadanand, Dwivedi, D.K.: Modeling of CZTSSe solar photovoltaic cell for window layer optimization. Optik (Stuttg) **222**, 165407–165419 (2020)

Sadanand, Dwivedi, D.K.: Modeling of photovoltaic solar cell based on CuSbS absorber for the enhancement of performance. IEEE Trans Electron Devices. **68**(3), 1121–1128 (2021)

Sadanand, Singh, P.K., Rai, S., Lohia, P., Dwivedi, D.K.: Comparative study of the CZTS, CuSbS2 and CuSbSe2 solar photovoltaic cell with an earth-abundant non-toxic buffer layer. Sol. Energy. **222**, 175–185 (2021)
Sahu, A., Garg, A., Dixit, A.: A review on quantum dot sensitized solar cells: Past, present and future towards carrier multiplication with a possibility for higher efficiency. Sol. Energy **203**, 210–239 (2020)
Sharma, A., Yadav, R.S., Pandey, B.P.: Performance analysis of PbS colloidal quantum dot solar cell at different absorption coefficient. J. Energy Environ. Sustain. **2019**(7), 32–35 (2019)
Sukharevska, N., et al.: Scalable PbS quantum dot solar cell production by blade coating from stable inks. ACS Appl. Mater. Interfaces **13**(4), 5195–5207 (2021)
Tripathi, S., Lohia, P., Dwivedi, D.K.: Contribution to sustainable and environmental friendly non-toxic CZTS solar cell with an innovative hybrid buffer layer. Sol. Energy **204**, 748–760 (2020)
Tvrdy, K., Kamat, P.V.: Quantum dot solar cells. Compr. Nanosci. Technol. **1–5**, 257–275 (2011)
Xing, M., Zhang, Y., Shen, Q., Wang, R.: Temperature dependent photovoltaic performance of TiO2/PbS heterojunction quantum dot solar cells. Sol. Energy **195**, 1–5 (2020)
Yasin, S., Al Zoubi, T., Moustafa, M.: Design and simulation of high efficiency lead-free heterostructure perovskite solar cell using SCAPS-1D. Optik Stuttg. **229**, 166258–166267 (2021)
Yuan, J., et al.: Metal halide perovskites in quantum dot solar cells: progress and prospects. Joule **4**(6), 1160–1185 (2020)
Zhang, Y., Ram, M.K., Stefanakos, E.K., Goswami, D.Y.: Synthesis, characterization, and applications of ZnO nanowires. J. Nanomater. **2012**, 1–22 (2012)